 doi:10.20944/preprints202205.0170.v1

Article

Reliable Machine Learning Model for Shear Strength of Reinforced Concrete Beams Strengthened Using FRP Jackets

Moamen Gasser [1], Omar Mahmoud [1] and Ahmed Deifalla [1,] *

[1] Future University in Egypt; diffalaf@mcmaster.ca.
* ahmed.deifalla@fue.edu.eg; Cell: (+2) 01021490978-Phone: (202) 26186100 Ext 1408-Fax: (202) 26186111.

Abstract: All over the world, externally bonded fiber-reinforced polymer systems used to strengthen concrete elements improve building sustainability. However, reports issued by the American Concrete Institute Committee 440 called for heavy scrutinizing before actual field implementation. The very limited number of proposed equations lacks reliability and accuracy. Thus, further investigation in this area is needed. In addition, machine learning techniques are being implemented successfully in developing strength models for complex problems. This study aims to provide a reliable machine learning model based on an experimental database. The proposed model was developed and validated against the experimental database and the very limited models in the literature. The model showed improved agreement with the experimental results compared to the previous models.

Keywords: Shear Strength, FRP, Anchorage devices, effective FRP strain.

1. Introduction

Significant shear act upon reinforced concrete (RC) elements in many buildings. Whittle reported failures in various RC buildings, and a few were related to shear [1]. The shear failure of RC beams is brittle [2-6]. The elevated cost of infrastructure replacement has prompted research into various strength and rehabilitation techniques. Shear strength is required in many projects [7]. The fiber-reinforced polymer (FRP) fabrics have many advantages over steel plates. Thus, research has been conducted to investigate the behavior of FRP externally and internally RC beams [10-12]. FRP has been used fruitfully in the aerospace and automotive industries for a few decades. It has been used for new structural elements in recent years, particularly in aggressive environments such as chemical plants, due to its high resistance to corrosion [13-16]. FRP can be used in situations where the usage of steel would be impossible or impractical [17-20]. For instance, it can be formed on-site to fit any irregular shape. FRP fabrics can be wrapped around curves (i.e., beams' sides, columns' corners, or beams' soffits). It is lighter in weight than steel with the same strength [21-23]. It is easy to handle and cut into the required length.

Worldwide, there is a lack of consensus on the shear strength contribution of the externally bonded (EB)-FRP reinforcement. Several design guidelines and codes exist worldwide [24-28]. This lack is due to the following reasons:

- The complexity of the shear phenomenon;
- The debonding failure of the external jackets for some configurations and its prediction;
- The linear behavior of the FRP material (the EB-FRP stirrups do not yield);
- The interaction between internal steel reinforcements, the concrete, and the EB-FRP reinforcement.

In addition, The EB-FRP shear strengthening can be performed in different configurations:

- Fully wrapping the sheets around the section (fully wrapped);
- Bonding L-shaped laminates or sheets to the bottom or the sides of the beam cross-section (U-shaped);
- Bonding sheets or laminates to the lateral sides of the cross-section (side-bonded).

The sheets and laminates can be bonded in a continuous or discontinuous configuration. However, both U-shaped and side-bonded configurations are susceptible to debonding once a critical shear crack opens and widens. Then, suppose the bonded length of each strip at the upper side of the crack (for the U - shaped) or at both sides of the crack (for the side - bonded case) is not long enough to anchor the tensile force the FRP. In that case, the laminate fails suddenly by debonding before ultimate capacity is reached. This type of failure mode can be eliminated by using anchorage devices as appropriate.

The beams' shear strength of beams strengthened using EB-FRP can be calculated as the summation of the shear contribution of the various components: concrete, transverse steel (if any), and EB-FRP. Some of the existing guidelines add the contribution of the EB-FRP reinforcement to the shear strength of the un-strengthened element [24-28]. However, previous studies have shown that EB-FRP jackets will affect the effective stress level of internal steel. Thus, this superposition approach could lead to nonconservative results [29-31]. This lack of conservative could be because it changes concrete diagonal cracking, the diagonal strut orientation, or the transverse reinforcement stress.

The engineering community is increasingly using EB-FRP systems to strengthen existing reinforced concrete (RC) structures. International recognition and widespread application of this method are primarily the results of extensive and valuable research efforts implemented in recent years. However, debonding of EB-FRP sheets has been a major issue for concrete structures strengthened in shear and torsion using EB FRP methods. For RC beams strengthened using EB-FRP, failure by debonding of EB-FRP is generally a brittle type of failure. Therefore, for such beams, debonding is an undesirable failure mode that should be avoided. There are two types of EB-FRP debonding were observed by Deifalla [21-23], namely, end or intermediate debonding, as shown in Figure1, which is generally caused by concrete cracking or cover spalling.

The primary obstacle presently preventing the widespread use of FRP anchorage measures is that no rational and reliable design rules currently exist. As a result, FRP design guidelines stipulate that representative experimental testing should substantiate the practical implementation of anchorage devices [24-28]. However, the guidelines do not specify the types of testing procedures considered adequate [32-34]. The repercussions of time and budget constraints on small- and large-scale industrial projects mean that such testing is rarely practiced. As a result, the potential benefits of FRP anchorages have typically been superseded by more conservative strength approaches such as section enlargement or column insertion. Although anchorage devices applied to the ends of FRP reinforcements have been tested by many researchers, the results have been limited by case dependency, with relatively small sample sizes being employed for each study.

The strength of EB-FRP strengthened RC beams is affected by the EB-FRP types, directions, distributions, and schemes. The effectiveness of EB-FRP is maximized by bonding the EB-FRP parallel to the direction of principal tensile stress. Therefore, EB-FRP schemes could result in the different shear capacities of EB-FRP RC beams. Detailed investigations on the shear strength of RC members have been relatively limited, and many questions regarding the shear strength mechanism are not yet settled. With the following exception, many researchers have idealized the EB-FRP materials as analogous to internal steel stirrups if the shear contribution of EB-FRP comes from the tensile fiber capacity at a strain close to the FRP ultimate tensile strain. Current design code provisions exist for EB-FRP elements, and many experimental tests have been carried out in this field of research.

If full FRP wrapping is not feasible, EB-FRP strengthened beams using FRP anchorage systems have been recently gaining attention, which can be used to achieve the

Preprints (www.preprints.org) | NOT PEER-REVIEWED | Posted: 12 May 2022 doi:10.20944/preprints202205.0170.v1

full design capacity of the FRP sheet [35-36]. The European fib [24] code recommends that FRP shear reinforcement be anchored to the compressive zone of the RC member. However, no further details were provided. In addition, the American Concrete Institute Committee 440 indicated that mechanical anchorages could be used at the termination points of FRP fabrics to develop larger tensile forces or increase stress transfer. However, the effectiveness of these mechanical anchorages and the level of tensile stress they can develop should be heavily scrutinized and substantiated through representative physical testing before field implementation [27]. In a study by Mofidi [35-37], it was concluded that more experimental results are needed to fully verify the calculated anchorage factors for the end-anchorage systems used in this research study. Kalfat [38] conducted a state-of-the-art review and concluded that strength improvement due to anchoring FRP materials had been demonstrated. However, there remains a lack of enough work in this area. A more recent review by Godat [39] has shown that further research is needed to enhance the reliability of the shear strength predictions of FRP -strengthened beams. The interaction between the FRP shear strength, strain, and parameters are required for robust design equations.

Machine learning is being implemented in various applications because it can capture the actual behavior for complex problems involving many parameters [40-41]. This research investigation aims at developing a reliable and accurate strength model based on advanced machine learning techniques. An extensive database was collected and used to train and validate the model, as shown in figure 2. A machine learning model was developed and compared with available models from the literature. Concluding remarks were outlined.

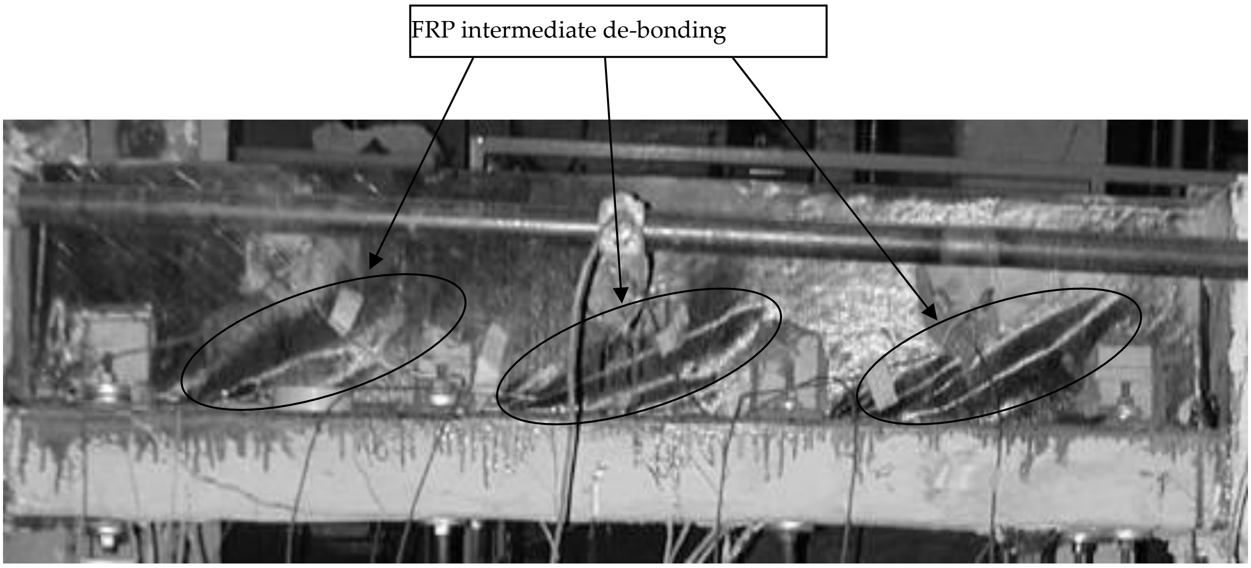

(a)

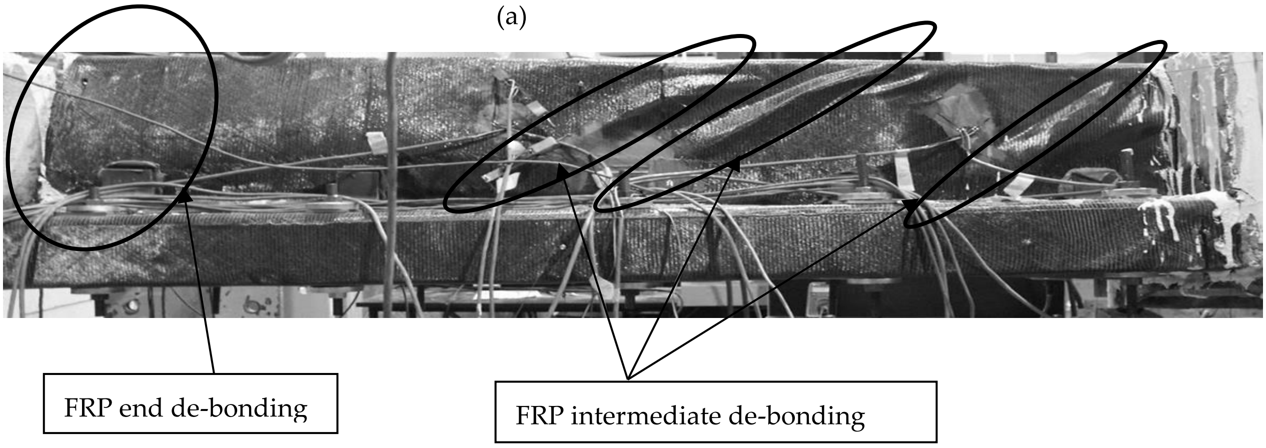

(b)

Figure 1. FRP end and intermediate debonding (courtesy of Dr. Deifalla).

2. Previous Studies

Relatively limited detailed studies have investigated the shear strength of RC members; in addition, many questions regarding the strength mechanism, especially the usage of anchorage devices, are yet to be resolved. Many researchers have idealized the EB-FRP jacket as similar to internal steel stirrups, assuming that the shear contribution of EB-FRP to shear capacity arises from the capacity of the FRP to carry tensile stresses at a strain, which is less than or equal to the FRP ultimate tensile strain [16-18]. Current Design Guidelines [24-28] are available for designing EB-FRP elements, and many experimental tests have been carried out in this field of research. Both empirical evidence and code indicate that a performance improvement can be attained; however, more detailed work is required to quantify their contribution to the shear strength of the beams [24-28]. Many parameters influence the effective FRP strain for shear strengthened RC members, including but not limited to: (1) The type of fibers in terms of Young's Modulus; (2) The fiber orientation in terms of the angle of inclination to the longitudinal axis of the beam; (3) The fiber distributions in terms of the number of plies and thickness of the FRP fabrics; (4) The FRP bond schemes in terms of the sides the FRP is bonded to (i.e., side bonding; U-jacket; full wrapping); (5) The concrete compressive strength; and (6) The usage of anchorage devices.

Preprints (www.preprints.org) | NOT PEER-REVIEWED | Posted: 12 May 2022 doi:10.20944/preprints202205.0170.v1

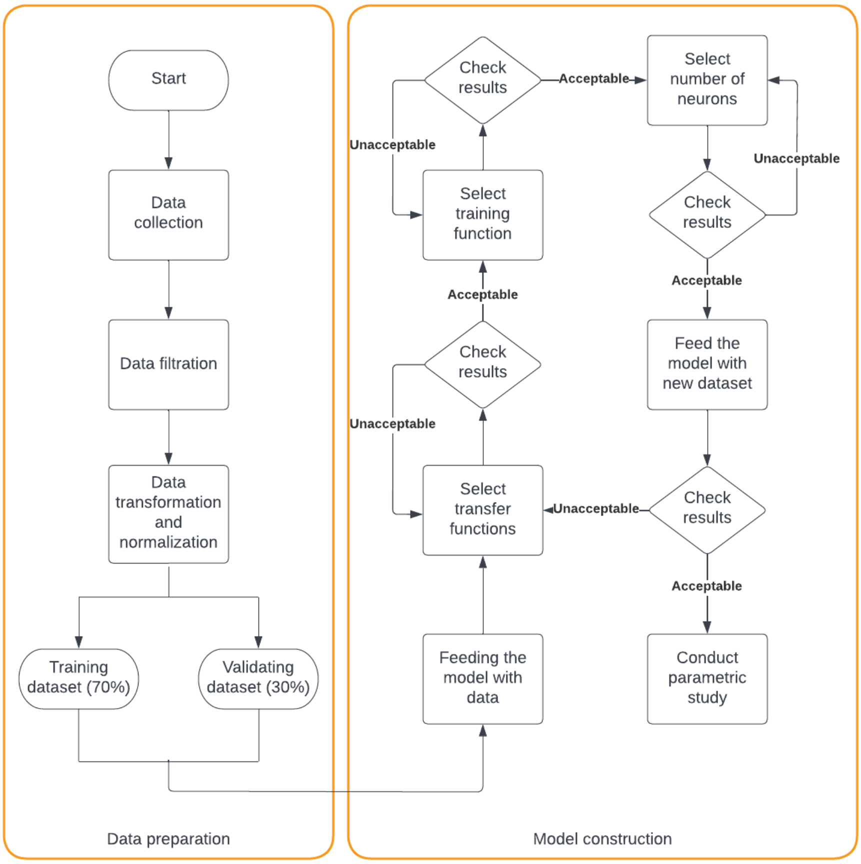

Figure 2. Work scheme.

3. Experimental database

An extensive database of 200 beams was strengthened using an EB-FRP jacket under shear collected from the literature. The database contains results from more than 80 experimental studies. In addition, this database includes Eb-FRP beams available in the literature [33, 42-44]. Although the data is available in existing databases, all data was validated using the original study.

Collected parameters were related to the beam and the FRP jacket as follows: Width of beam cross-section (X1), beam height (X2), the effective depth of beam cross-section (X3), beam span (X4), shear span to depth ratio (X5), concrete compressive strength (X6), steel flexure reinforcement ratio (X7), and steel shear reinforcement ratio (X8), strength technique (X9), FRP jacket height (X10), the width of FRP jacket (X11), the thickness of FRP jacket (X12), spacing between FRP strips (X13), FRP reinforcement ratio (X14), angle of fiber orientation (X15), ultimate stress of FRP (X16), FRP young's modulus (X17), and FRP rupture strain (X18), and Shear strength in kN (X19). Table 1 shows the statistical measures for all parameters.

Preprints (www.preprints.org) | NOT PEER-REVIEWED | Posted: 12 May 2022 doi:10.20944/preprints202205.0170.v1

Table 1. Statistical measures for all parameters.

	Minmum	Maximum	Average	Stdev.
X1	70	600	189	84
X2	102	720	336	119
X3	85	660	291	107
X4	600	6400	2205	1012
X5	1.3	6.9	2.85	0.74
X6	4	63.4	27.37	11.16
X7	0.75	7.54	2.89	1.41
X8	0.02	0.84	0.10	0.14
X10	89	720	319	121
X11	1	300	47	75
X12	0.044	4000	223	575
X13	1	500	99	134
X14	0.0029	0.0895	0.0042	0.0084
X15	20	90	80	19
X16	112	4840	3112	1108
X17	5	392	202	85
X18	6.6	47.4	16.6	6.3
X19	3	494	69	64

3. Parameters selection

Pearson parametric method was used to determine the influence of beam details on the FRP shear strength, as shown in figure3. The selected parameters included X1, X2, and X3, while parameters X4, X5, X6, X7, and X8 were not chosen as they have a lower Pearson coefficient. For a more efficient and faster training and validating process, the input parameters have been normalized to be between 0 and 1, according to equation 1. While FRP's shear strength (model's output) has been transformed according to equation 2 for better output distribution, as shown in figure4.

- $$X_{i,norm} = \frac{X_i - X_{avg}}{X_{max} - X_{min}} \qquad 1. \qquad (1)$$

where i is the number index for each input parameter, $X_{i,norm}$ is the normalized value for the input parameter, X_i is the value of the input parameter before normalization, Xavg is the average of the parameter X_i, X_{max} and X_{min} are the values of the maximum and minimum values of the input parameter X_i.

- $$S^T = ln(S + 1) \qquad 2. \qquad (2)$$

where S is the value of the added shear strength by FRP in kN while S^T is its transformed value, the input parameter for the proposed model data has been filtered and transformed to follow a normal distribution curve for a better training process to build the model has been as shown in figure 4.

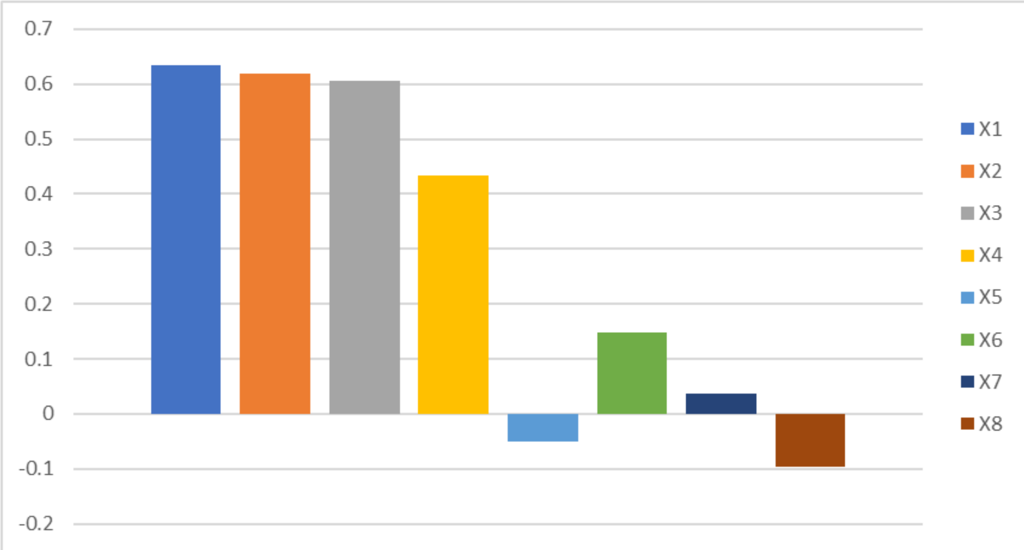

Figure 3. Results of Pearson variables study on FRP shear strength.

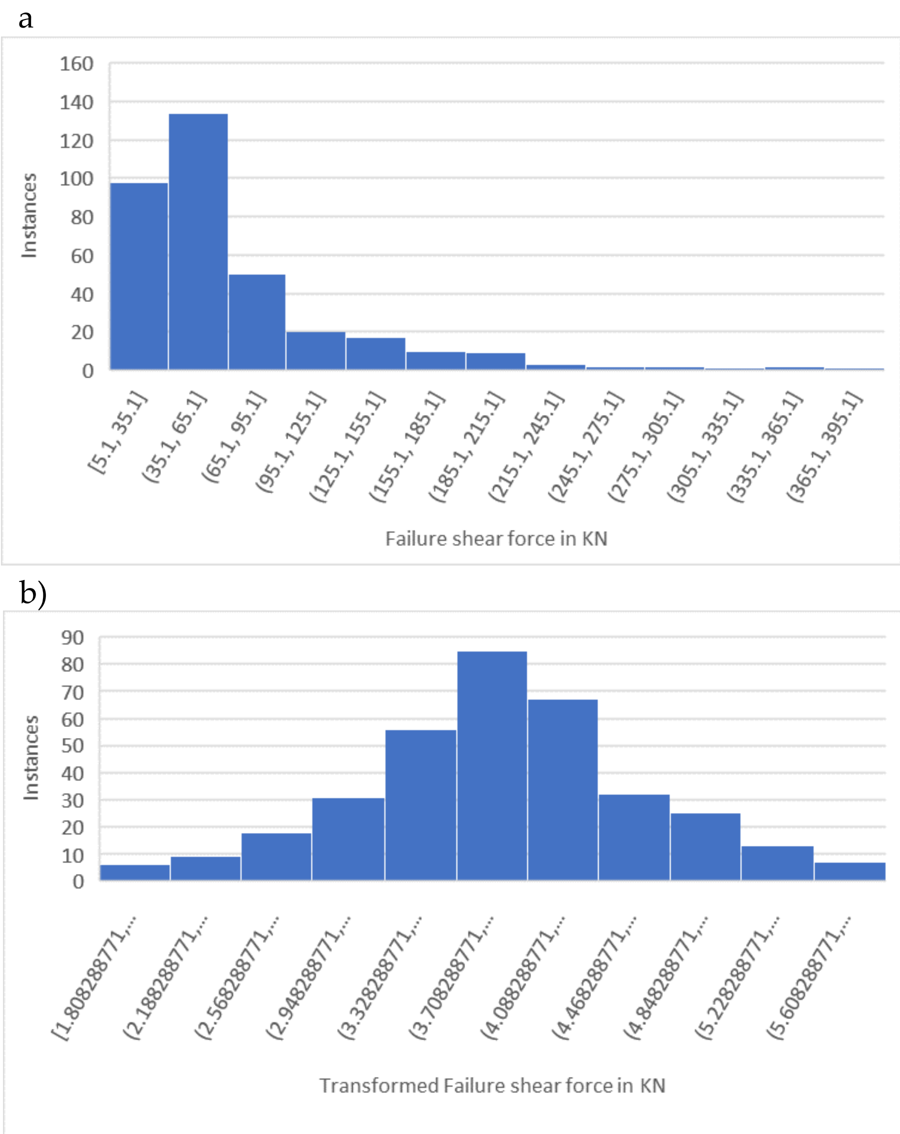

Figure 4. Distribution of the failure shear force a) before and b) after transformation.

Preprints (www.preprints.org) | NOT PEER-REVIEWED | Posted: 12 May 2022 doi:10.20944/preprints202205.0170.v1

4. Model development

A script has been developed to generate more than 6750 different artificial neural networks (ANN) models to compare and boost the developed model performance using MATLAB. In addition, different combinations of various parameters have been tested as shown if figure 5.

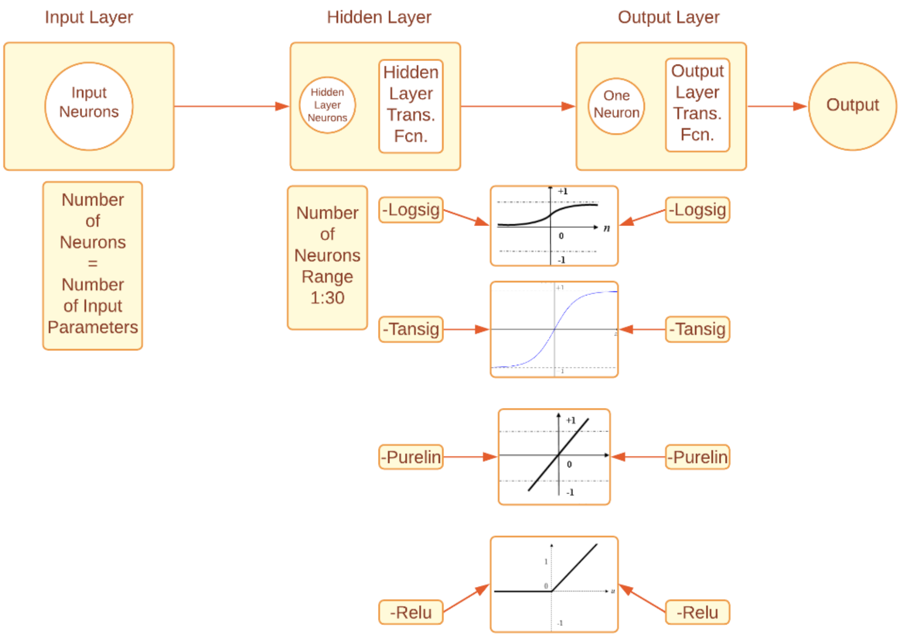

Figure 5. Combination of different model parameters.

During the model construction, the transfer function of the hidden and output layers were the first parameters to be determined. Then, the training function and the number of neurons in the hidden were optimized by plotting the number of neurons versus the correlation coefficient (R^2) and root mean square error (RMSE) in figures 6 and 7.

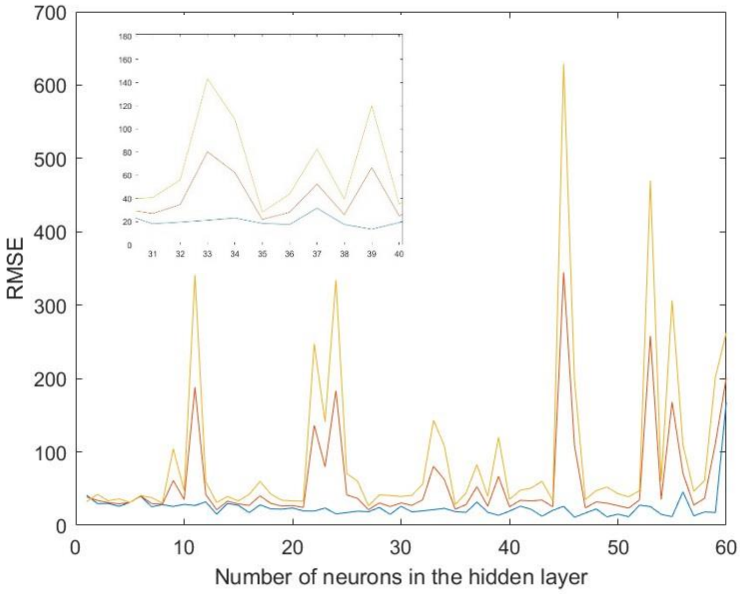

Figure 6. Neurons number in hidden layer versus RMSE.

Preprints (www.preprints.org) | NOT PEER-REVIEWED | Posted: 12 May 2022 doi:10.20944/preprints202205.0170.v1

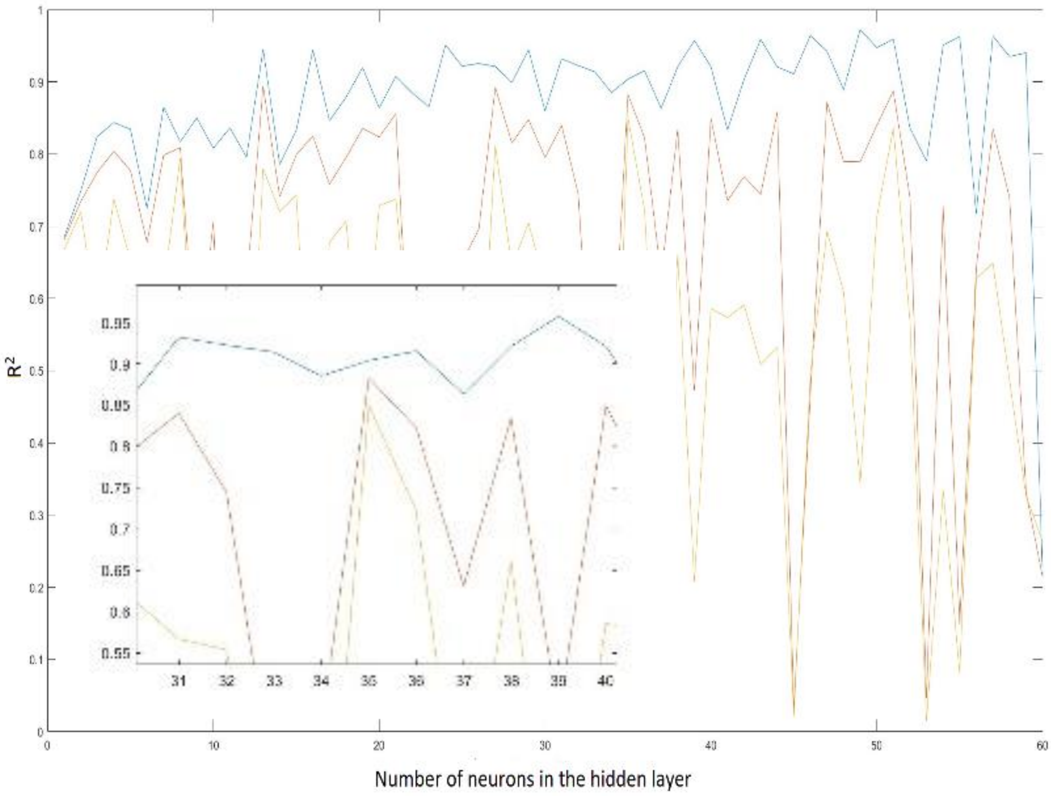

Figure 7. Neurons number in the hidden layer versus R^2.

The number of neurons was optimized to be 35 neurons in the hidden layer, while the transfer functions were TANSIG and PURELIN for the hidden and the output layers, respectively figure 8. Based on the constricted model, a mathematical equation has been developed to predict the shear strength added by FRP equation 3.

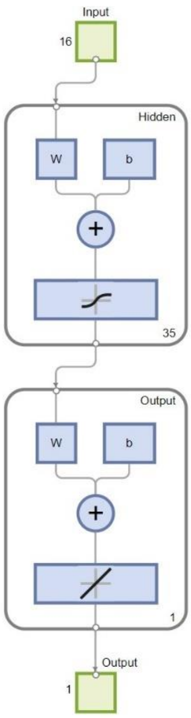

Figure 8. The proposed ANN model architecture.

- $$S = Exp\left[PURELIN\left[\sum_{i=1}^{N} W_{2i} TANSIG\left(\sum_{j=1}^{J} W_{1j} \times \frac{X_j - X_{avg}}{X_{max} - X_{min}} + b_{1i}\right)\right] + b_2\right] - 1 \quad 3. \qquad (3)$$

where Exp is the exponential function, N is the number of neurons in the hidden layer, which has been optimized to be 35 neurons, W2i is the weight of the output layer, J is the number of input variables, W1 is the weight of the hidden layer, Xj is the value of the input variable (strength configuration, X1, X2, X3, X9, X10, X11, X12, X13, X14, X15, X16, X17, and X18) b1 is the bias of the hidden layer, and b2 is the bias of the output layer.

Later, the performance of the ANN model was boosted by 1000 epochs; the best model outcome was found to be at the 8th epoch, then the validation check stopped the training process at the 14th epoch, as shown in figure 9.

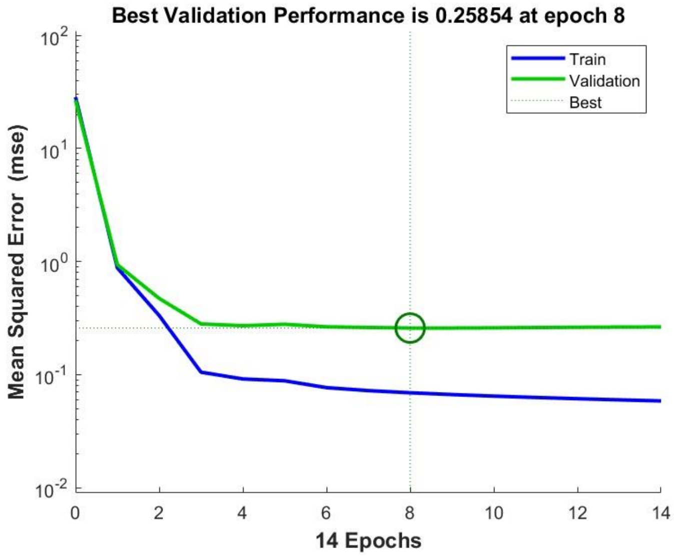

Figure 9. Epochs versus Mean square error.

5. Model validation

After the model construction, the model was used to predict the shear strength for FRP in KN then the predicted value was plotted versus the actual values in figure10. In addition, statistical tests have been conducted to test the accuracy of the newly developed model. Training, validating, and overall datasets have been evaluated using average relative error (ARE), average absolute relative error (AARE), relative deviation (RD), standard deviation (SD), RMSE, and R2 according to equations 3-8. Also, a comparison between the actual and the predicted values are presented in figure 11. Moreover, the ratio between the predicted and actual values has been calculated according to equation 9 for both the training and validating datasets and presented in figure 13.

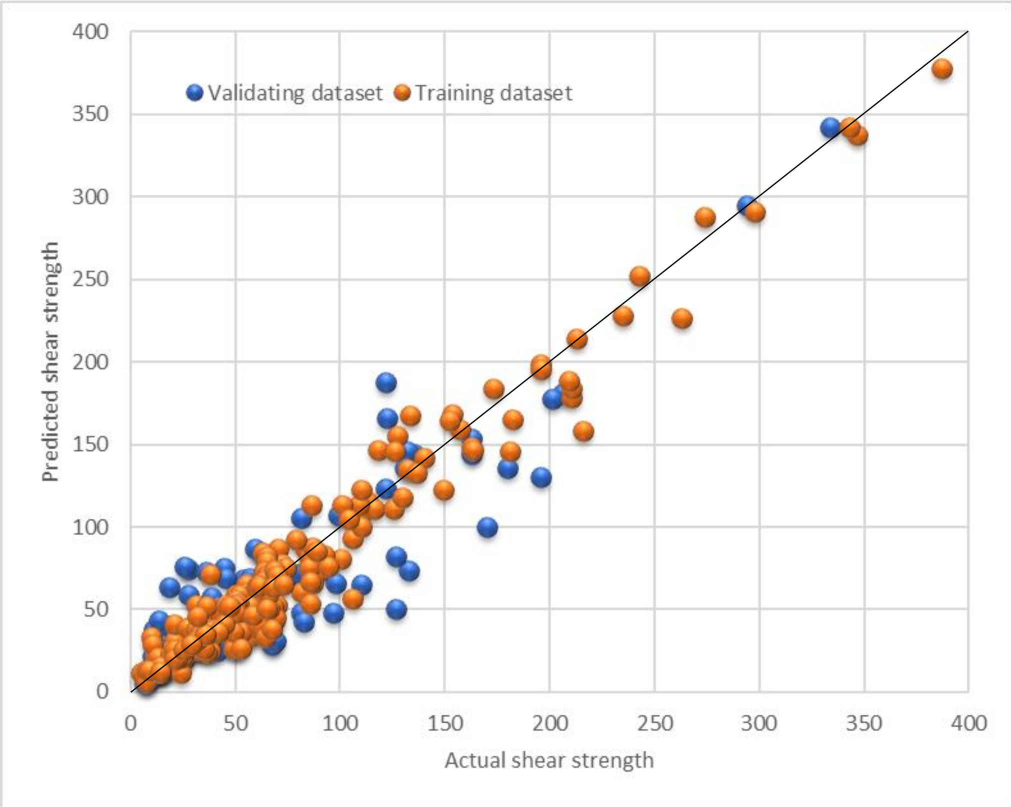

Figure 10. Actual Versus predicted shear strength value in kN.

- $$ARE = \left(\frac{1}{N} \times \sum_{i=1}^{N} \frac{S^{Predicted} - S^{Actual}}{S^{Actual}}\right) \times 100$$ 4. (4)

- $$AARE = \left(\frac{1}{N} \times \sum_{i=1}^{N} \left|\frac{S^{Predicted} - S_i^{Actual}}{S_i^{Actual}}\right|\right) \times 100$$ 5. (5)

- $$RD = \frac{S^{Predicted} - S^{Actual}}{S^{Actual}} \times 100$$ 6. (6)

- $$SD = \left\{\frac{1}{N-1} \times \sum_{i=1}^{N} \left(\frac{S^{Predicted} - S^{Actual}}{S^{Actual}}\right)^2\right\}^{0.5}$$ 7. (7)

- $$RMSE = \left\{\frac{1}{N} \times \sum_{i=1}^{N} (S^{Predicted} - S^{Actual})^2\right\}^{0.5}$$ 8. (8)

- $$R^2 = 1 - \frac{\sum_{i=1}^{N} (S^{Predicted} - S^{Actual})^2}{(S_{Actual}^{Mean} - S^{Actual})^2}$$ 9. (9)

- $$Ratio = \frac{F^{Predicted}}{F^{Actual}}$$ 10. (10)

where N is the number of tested data points, $S^{Predicted}$ is the predicted shear strength value in kN, S^{Actual} is the corresponding actual shear strength value in kN, and S_{Actual}^{Mean} is the average of the actual shear strength value in kN.

a)

 doi:10.20944/preprints202205.0170.v1

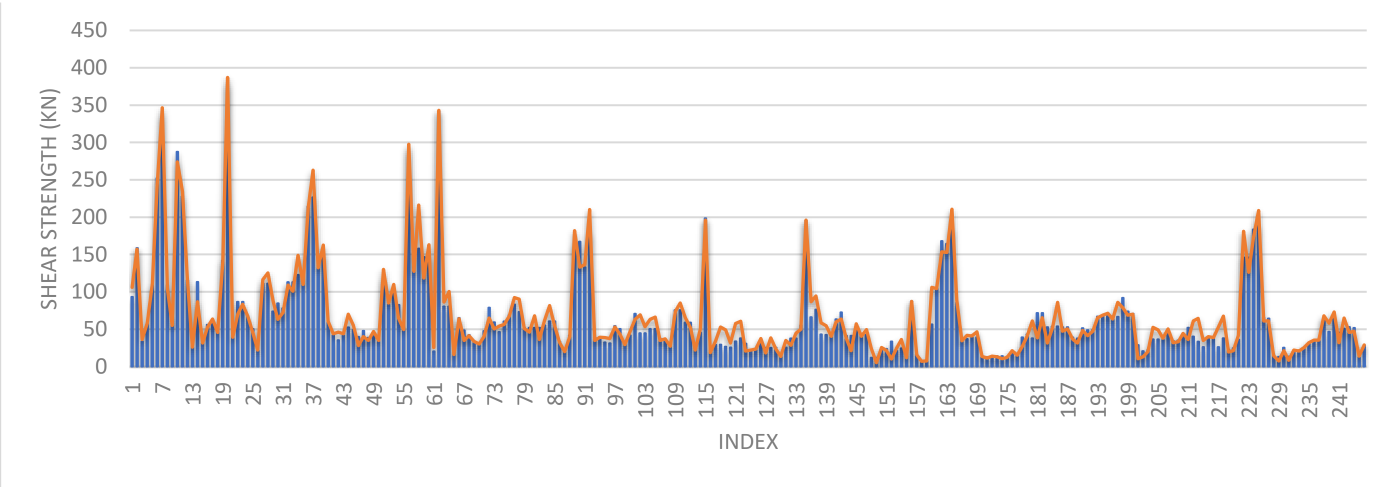

b)

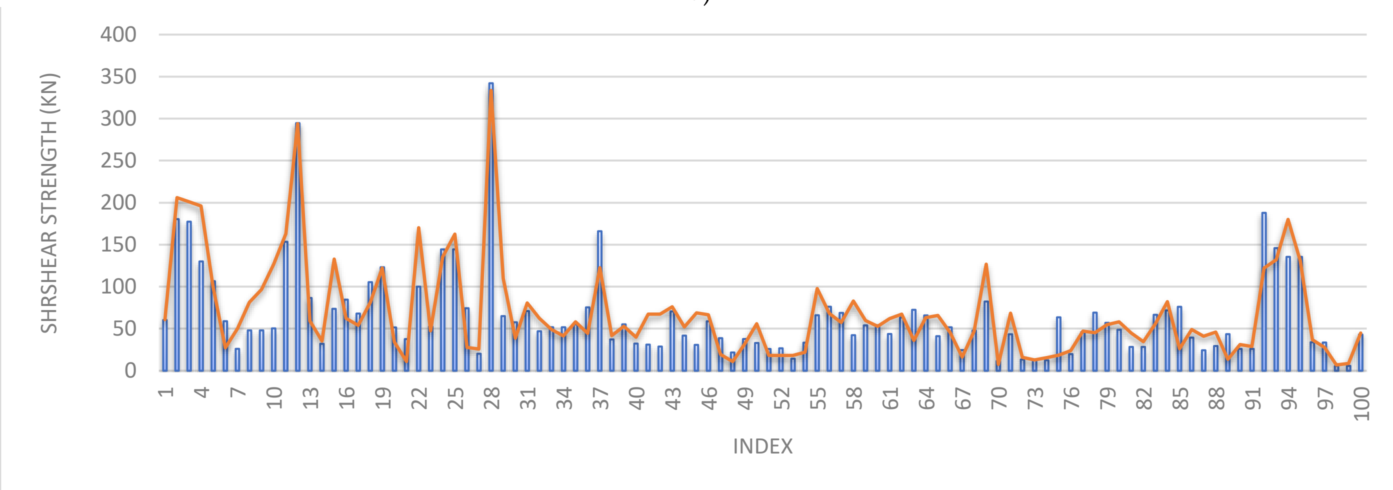

c)

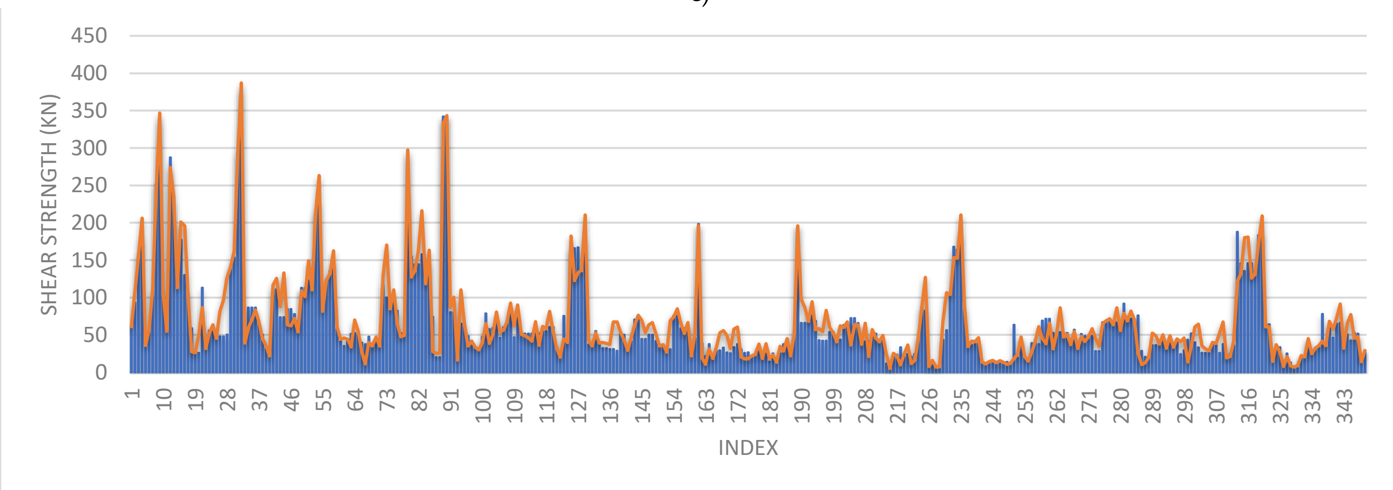

Figure 11. Comparing the actual and predicted shear strength values in kN for a) training dataset, b) validating c) overall datasets.

Preprints (www.preprints.org) | NOT PEER-REVIEWED | Posted: 12 May 2022 doi:10.20944/preprints202205.0170.v1

a)

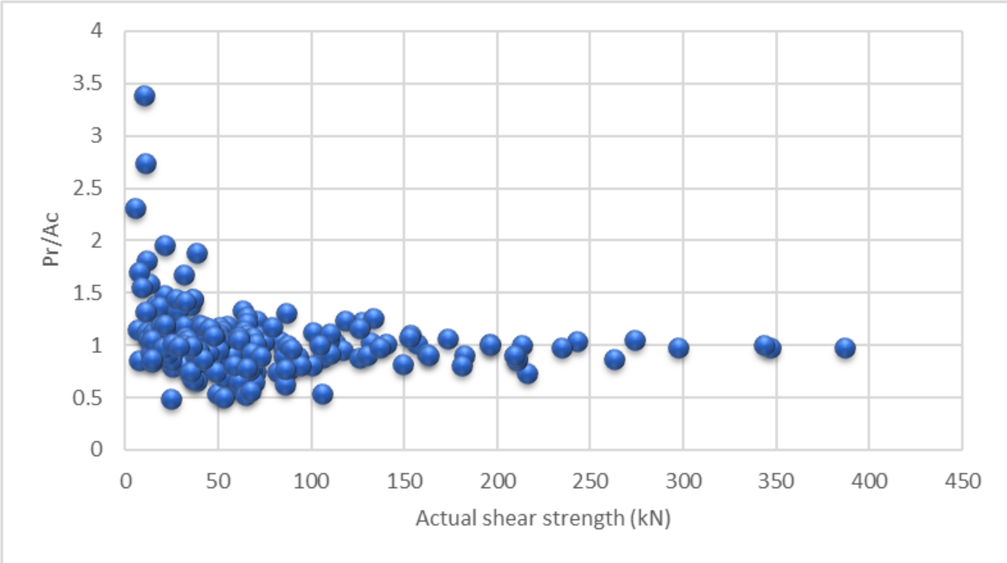

b)

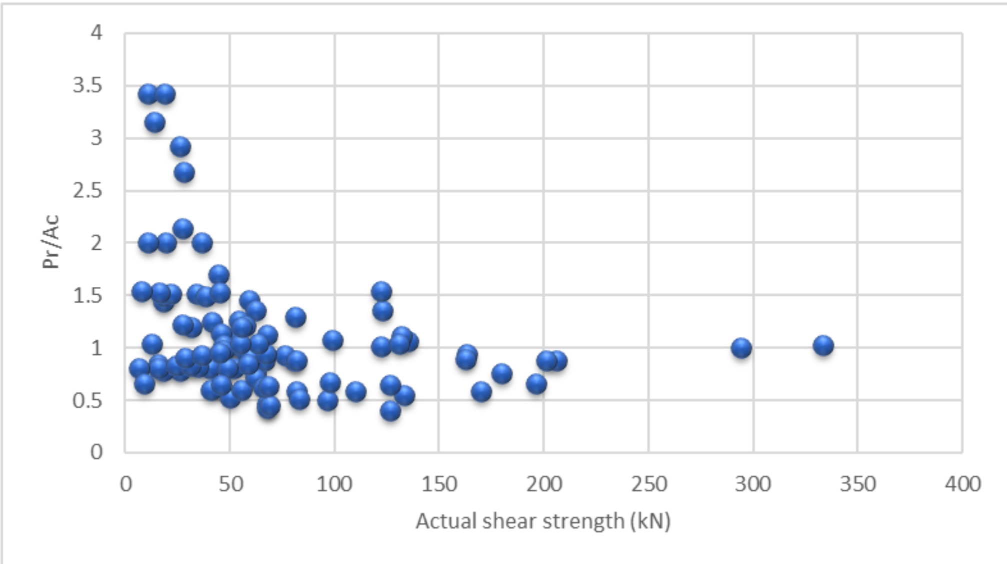

Figure 12. The ratio between predicted to actual shear strength versus the actual shear strength value in kN for a) training dataset and b) validating dataset.

The model showed excellent performance as it has R^2 and RMSE of 0.91 and 17.45 for the overall dataset, respectively. The R^2, RMSE, ARE, AARE and SD statistical tests are summarized and listed in figures 13-17, respectivelyIn addition, the results of the different datasets were compared to check the fitting of the proposed model. While RD is plotted versus the actual shear strength and presented in figure 18.

 doi:10.20944/preprints202205.0170.v1

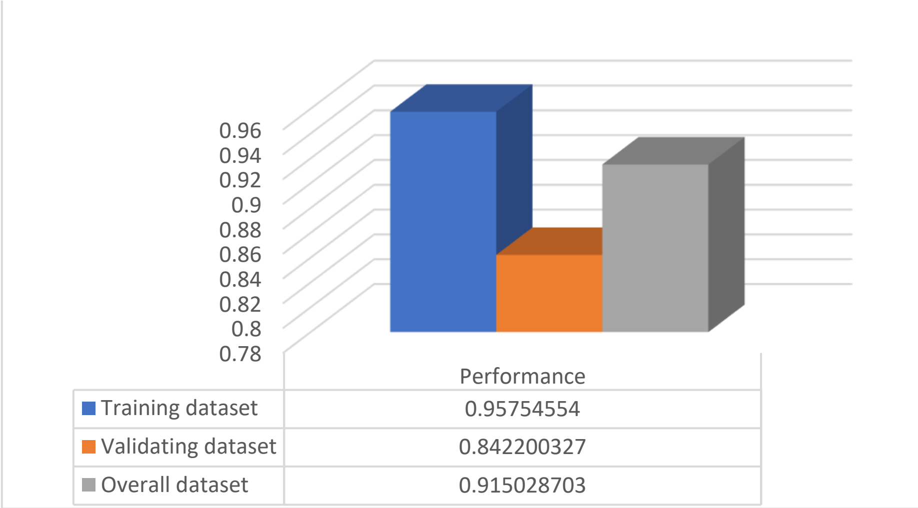

Figure 13. R^2 for training, validating, and overall datasets.

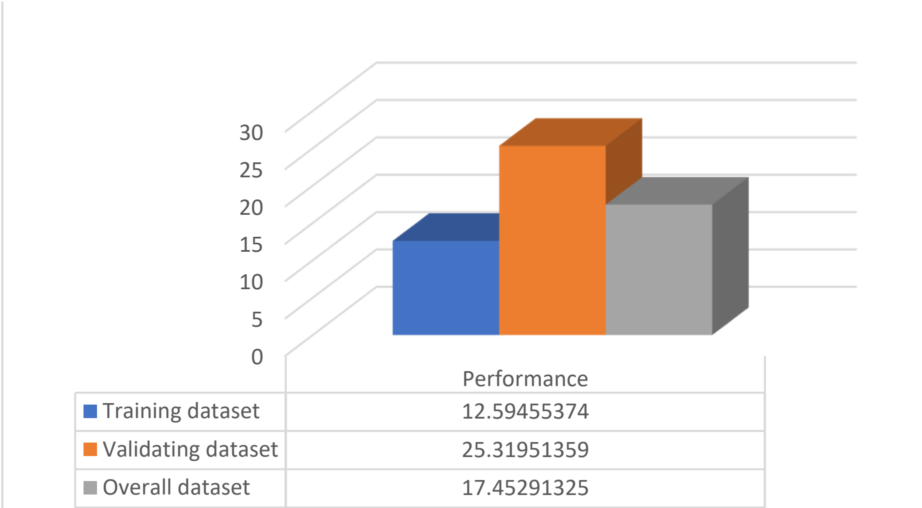

Figure 14. RMSE for training, validating, and overall datasets.

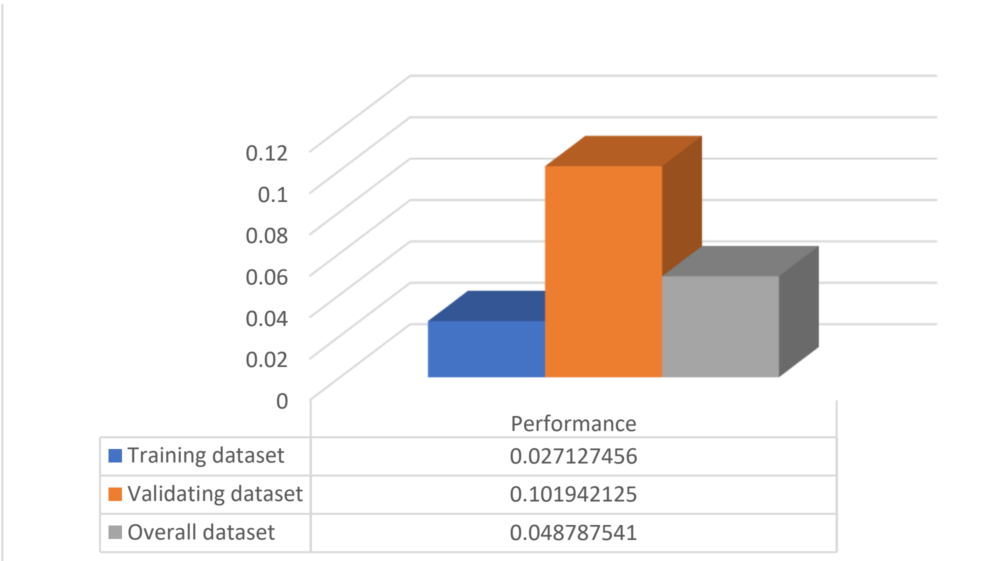

Figure 15. ARE for training, validating, and overall datasets.

Preprints (www.preprints.org) | NOT PEER-REVIEWED | Posted: 12 May 2022 doi:10.20944/preprints202205.0170.v1

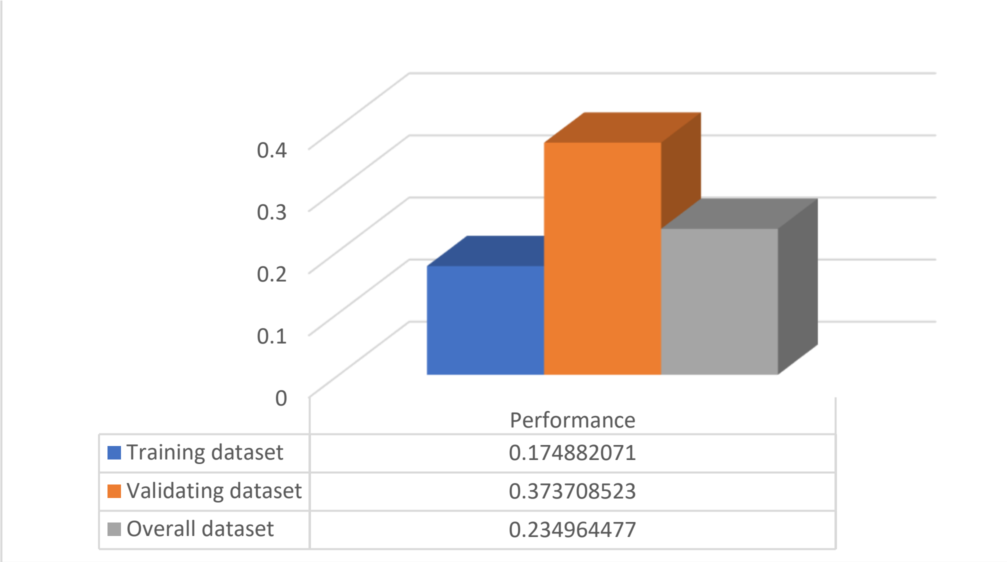

Figure 16. AARE for training, validating, and overall datasets.

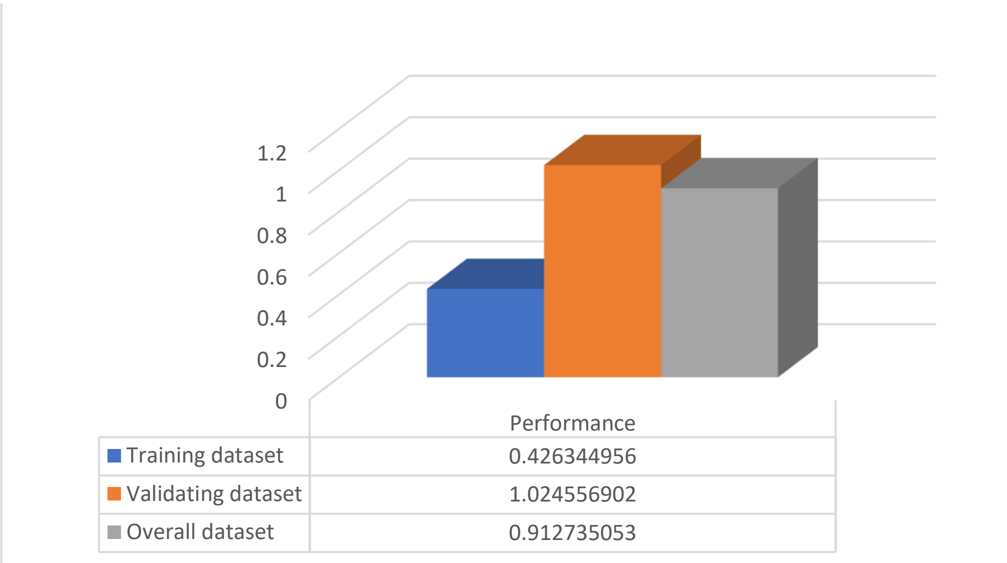

Figure 17. SD for training, validating, and overall datasets.

 doi:10.20944/preprints202205.0170.v1

a)

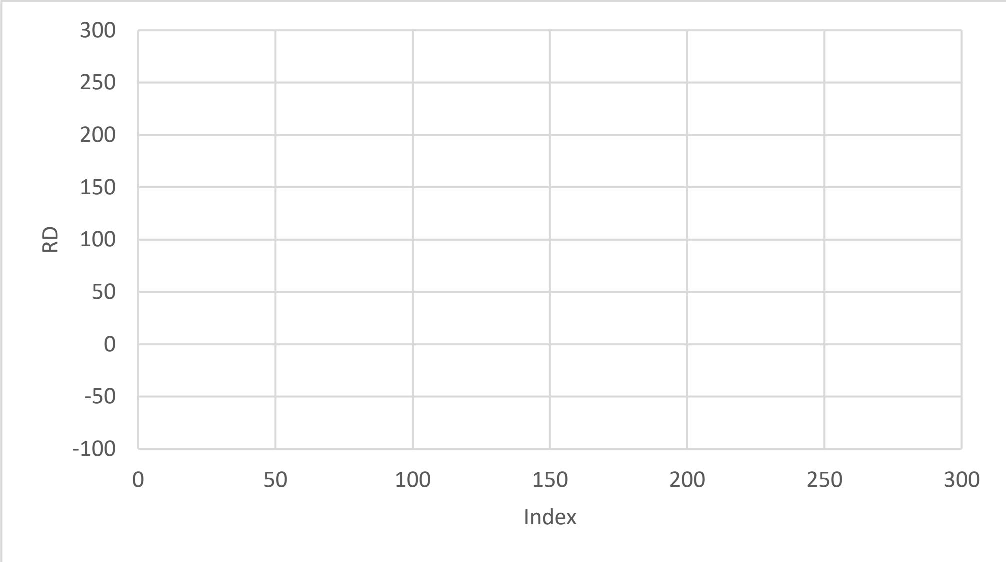

b)

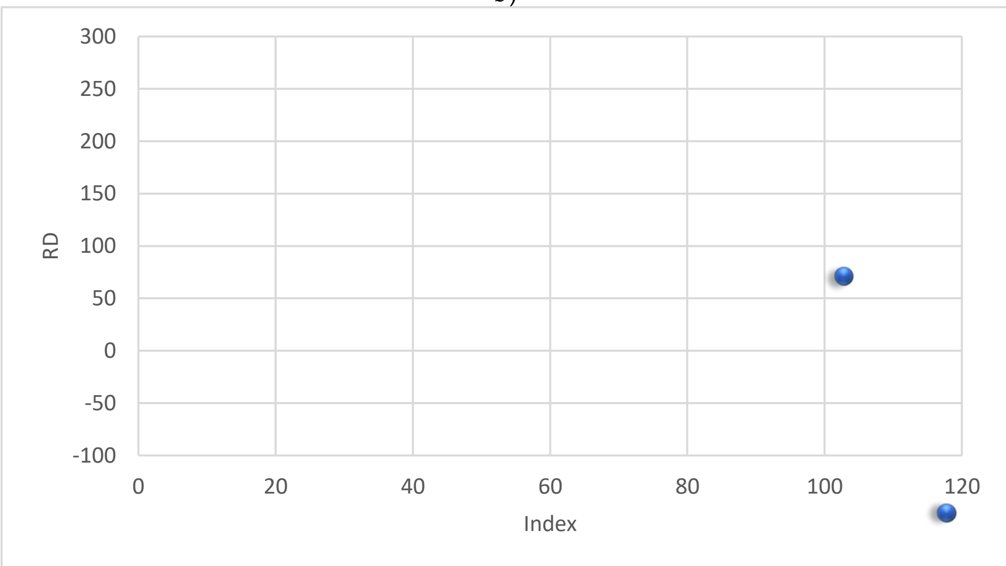

Figure 18. RD versus the testing point index for a) training b) validating datasets.

After validating the model and demonstrating its credibility in predicting the shear strength value added by the FRP, the model was then used to conduct a parametric study to study the impact of each parameter individually. When investigating a certain parameter, the rest of the variables were set constant at their average value while changing the value of the tested parameter. X10, X14, X15, and X17 were investigated, and their values are plotted versus the model outcome figures 19-22.

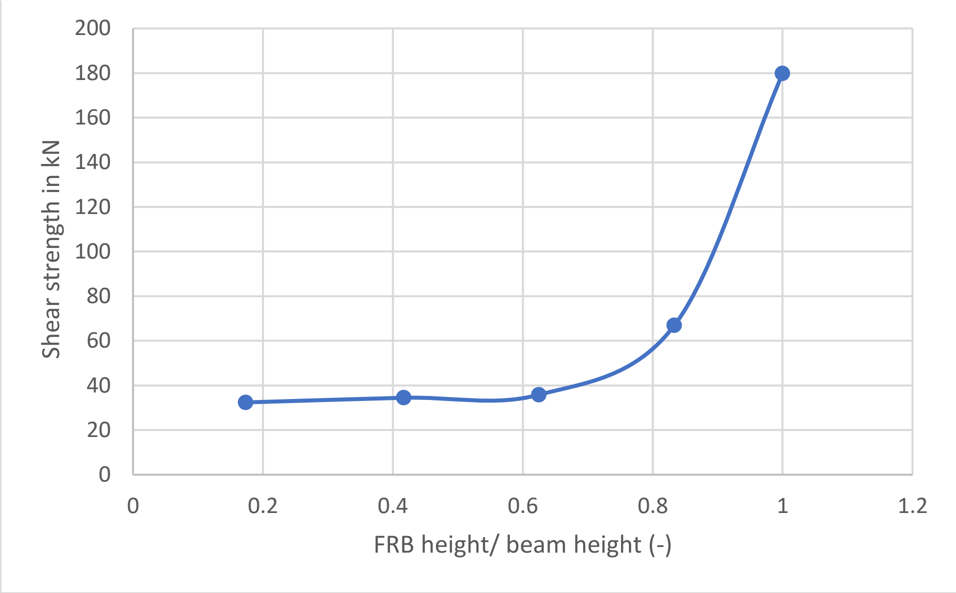

Figure 19. The effect of X10 on shear strength value.

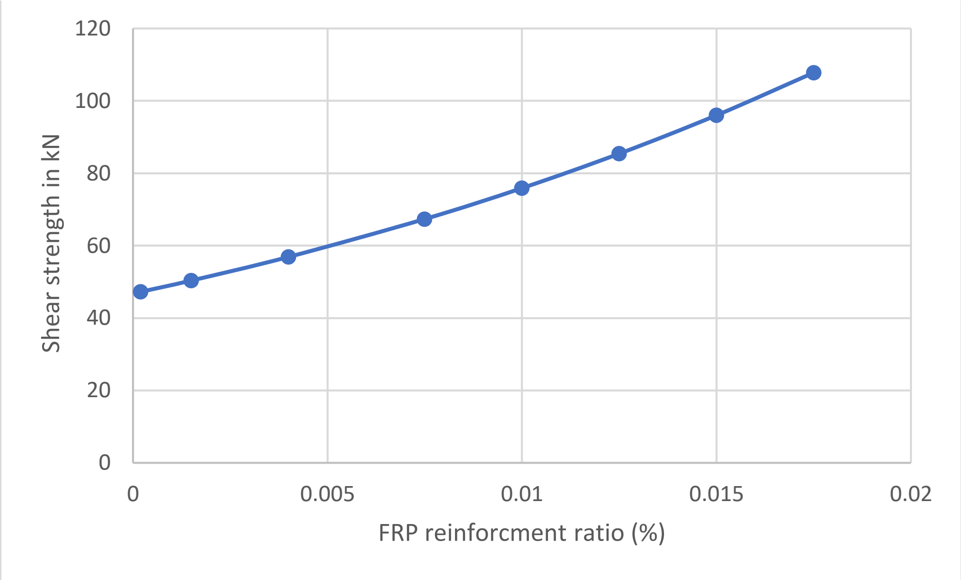

Figure 20. The effect of X14 on the shear strength.

Preprints (www.preprints.org) | NOT PEER-REVIEWED | Posted: 12 May 2022 doi:10.20944/preprints202205.0170.v1

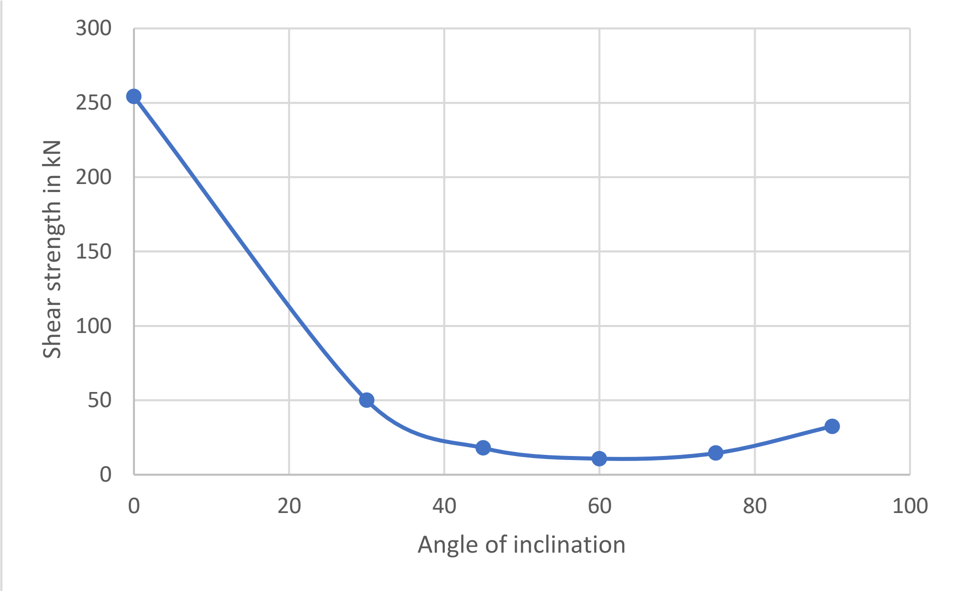

Figure 21. The effect of X15 on shear strength value.

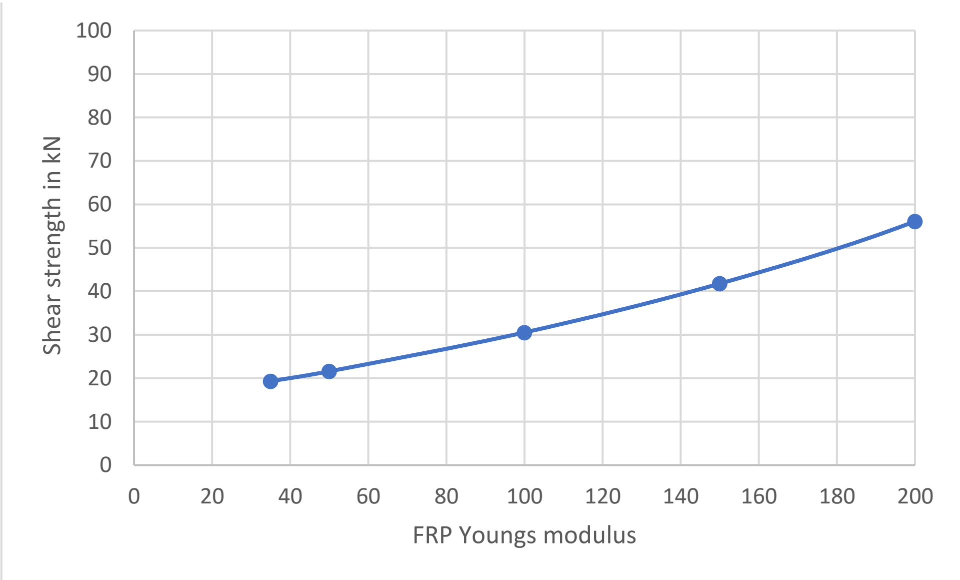

Figure 22. The effect of X17 on shear strength value.

6. Comparisons between the proposed model and existing machine models

In 2020 machine learning was used to predict the FRP shear strength capacity with a certain accuracy [46]. In this work, the proposed model performance has been evaluated and compared to the models from the literature. R^2 is one of the essential statistical parameters that can determine the accuracy of any model regardless of the values of the used data. R^2 for the overall datasets and the number of data used in developing the new model have been compared with their corresponding values from the previous model, as shown in figure23. The model from this work was constructed using a larger number of dataset points, giving the model a wide range of applicability. In addition, R^2 shows better performance and more accurate results than the models from the literature for all datasets.

Preprints (www.preprints.org) | NOT PEER-REVIEWED | Posted: 12 May 2022 doi:10.20944/preprints202205.0170.v1

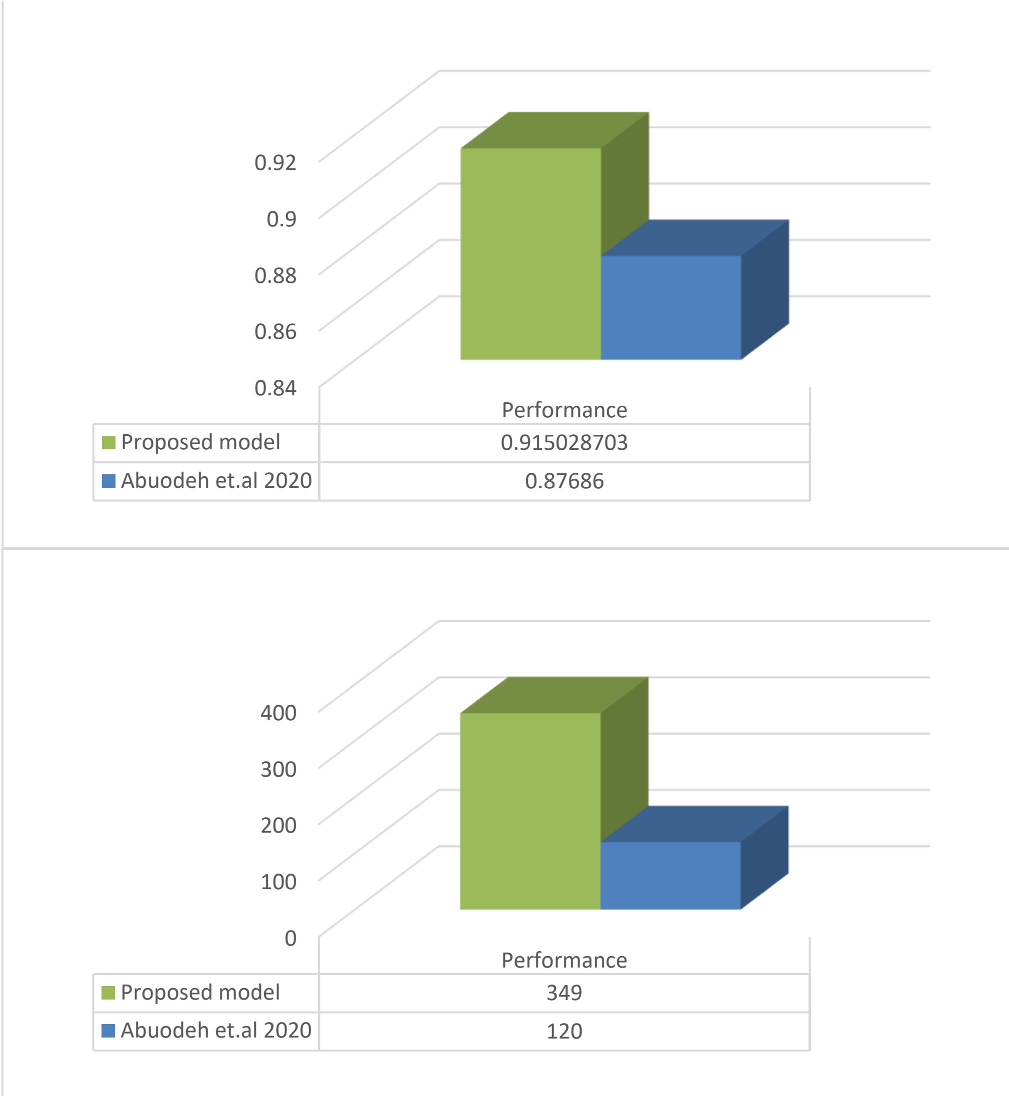

Figure 23. Comparison between the existing models from literature and the proposed model, based on a) R^2 and b) number of data points used.

7. Comparison between the existing design codes and guidelines and the proposed model.

Table 2 shows the statistical measures for various selected models' safety ratios, namely average and coefficient of variation. The safety ratio was defined as the ratio between the measured and the calculated FRP contribution. At the same time, selected models include the proposed model, the Fib 90 [19], the ACI [20], the CNR [21], the TR-55 [22], and the JSCE [23]. The proposed model captured the behavior of FRP strengthened beams and precited the FRP contribution accurately and consistently. The average ranged from 0.98 to 1.14, and the coefficient of variation ranged between 24% to 36%. While the selected models' average ranged between 0.48 to 4.46, and the coefficient of variation ranged between 35% to 95%.

Table 2. Statistical measures for proposed and selected model's a/d ≥ 2.5.

Scheme	Steel stirrups	Continuity	Proposed model		Fib 90		ACI		CNR		TR-55		JSCE	
			SR	C.O.V.	SR	C.O.V.	SR	C.O.V.	SR	C.O.V.	SR	C.O.V.	SR	C.O.V.
Wrapped	Without	Strips	0.98	24%	2.91	49%	3.85	58%	3.00	54%	3.85	58%	1.14	47%
		Continuous	1.14	33%	2.07	38%	-	-	2.15	38%	4.46	59%	0.93	37%
	With	Strips	0.98	24%	1.77	37%	2.32	49%	2.52	42%	2.49	44%	0.88	43%
		Continuous	1.14	33%	0.83	39%	-	-	1.03	43%	1.27	58%	0.43	33%
U-jacket	Without	Strips	1.08	31%	1.50	51%	1.64	64%	1.72	53%	1.58	49%	0.62	46%
		Continuous	1.07	36%	1.12	35%	-	-	1.05	43%	1.07	36%	0.45	36%
	With	Strips	1.08	31%	0.85	87%	1.23	62%	1.20	81%	1.10	68%	0.38	95%
		Continuous	1.07	36%	0.53	45%	-	-	0.51	43%	0.52	46%	0.19	44%
One side	Without	Strips	1.00	29%	-	-	1.34	73%	-	-	1.05	72%	0.74	51%
		Continuous	1.08	30%	-	-	-	-	-	-	0.91	49%	0.84	40%
	With	Strips	1.00	29%	-	-	1.15	72%	-	-	0.71	37%	0.61	47%
		Continuous	1.08	30%	-	-	-	-	-	-	0.41	41%	0.48	52%

8. Conclusions

MATLAB script has been developed to create 6750 different ANN models to compare and optimize the model performance. The model can predict the shear strength added value of FRP knowing the Width of beam cross-section, beam height, the effective depth of beam cross-section, strength technique, FRP jacket height, the width of FRP jacket, the thickness of FRP jacket, spacing between FRP strips, angle of fiber orientation, ultimate stress of FRP, FRP young's modulus, and FRP rupture strain. The input and output data have been adjusted to give a more efficient and faster training process. The model's accuracy has been measured using several statistical tests. R^2, RMSE, ARE, AARE, and SD was found to be 0.91, 17.45, 0.048, 0.23, and 0.91, respectively, for the overall dataset. A parametric study has been conducted to study the influence of the FRP jacket height, the width of the FRP jacket, the thickness of the FRP jacket, spacing between FRP strips, angle of fiber orientation, ultimate stress of FRP, FRP young's modulus, and FRP rupture strain. A comparison between the newly developed model and the model from previous work has been made. The comparison showed that the proposed model has better accuracy, and the number of datasets used in this research is larger than in the other work.

8. Patents

This section is not mandatory but may be added if there are patents resulting from the work reported in this manuscript.

Supplementary Materials: Not applicable.

Author Contributions: Conceptualization, Gasser and Omar.; methodology, Gasser and Omar.; software, Gasser and Omar.; validation, Gasser and Omar.; resources, Deifalla.; data curation, Deifalla.; writing—original draft preparation, Gasser and Omar.; supervision, Deifalla.; project administration.

Funding: This research received no external funding.

Data Availability Statement: Not applicable.

Acknowledgments: Not applicable.

Conflicts of Interest: The authors declare absoluely no conflict in the interest

References

1. Whittle, R. Failures in Concrete Structures—Case Studies in Reinforced and Prestressed Concrete; FL 33487-2742; CRC Press: Boca Raton, FLorida, USA; Taylor and Francis Group, Abingdon, UK, 2013; 140 pp.
2. Chalioris C. E..; Karayiannis C. Effectiveness of the use of Steel fibres on the Torsional behavior of Flanged concrete beams. Cement Concrete Composites. 2009, 31, 331–341.
3. Deifalla A.; Awad A.; Seleem H.; AbdElrahman A. Experimental and Numerical Investigation of the Behavior of LWFC L-girders under Combined torsion. Structures 2020, 26, 362–77. https://doi.org/10.1016/j.istruc.2020.03.070.
4. Deifalla A., Awad A.; Seleem H.; AbdElrahman A. Investigating the Behavior of lightweight foamed concrete T-Beams under Torsion, Shear, and Flexure. Eng. Struct. 2020, 219, 110741. https://doi.org/10.1016/j.engstruct.2020.110741.
5. Deifalla A.; Ghobarah A. Behavior and Analysis of Inverted T-shaped RC beams under Shear and Torsion. Eng. Struct. 2014, 62, 776–786.
6. G. Karayannis, C.; K. Kosmidou, P.-M.; E. Chalioris, C. Reinforced Concrete Beams with Carbon-Fiber-Reinforced Polymer Bars—Experimental Study. Fibers 2018, 6, 99. https://doi.org/10.3390/fib6040099.
7. Gosbell T.; Meggs, R. West gate bridge approach spans FRP strengthening Melbourne. In Proceedings of the IABSE Symposium, Melbourne, Australia, 11–13 September 2002.
8. FIB. FRP Reinforcement in RC Structures; Technical Report Prepared by a Working Party of Task Group 9.3; FIB Bulletin 40; International Federation for Structural Concrete: Lausanne, Switzerland, 2007; p. 151.
9. Oller E., Kotynia R., Antonio Marí A. Assessment of the existing models to evaluate the shear strength contribution of externally bonded frp shear reinforcements. Composite Structures 264 (2021) 113641.https://doi.org/10.1016/j.compstruct.2021.113641.
10. Kotynia, R., Oller, E., Marí, A., Kaszubska, M. Efficiency of shear strengthening of RC beams with externally bonded FRP materials – State-of-the-art in the experimental tests. Composite Structures 267 (2021) 113891. https://doi.org/10.1016/j.compstruct.2021.113891.
11. De Lorenzis, L., and Nanni, A., Shear strength of reinforced concrete beams with FRP rods, J. Comp. Constr., 2001, 5(2), 114–121.
12. Deifalla A. Refining the Torsion Design of Fibered Concrete Beams Reinforced with FRP using Multi-variable Non-linear Regression Analysis for Experimental Results. Eng. Struct. 2020, 224, 111394.
13. Deifalla, A. Torsion Design of Lightweight Concrete Beams without or with Fibers: A comparative study and a refined cracking torque formula. Structures 2020, 28, 786–802. https://doi.org/10.1016/j.istruc.2020.09.004.
14. Deifalla, A. Torsional Behavior of Rectangular and Flanged Concrete Beams with FRP Reinforcements. J. Struct. Eng. 2015, 141, 04015068.
15. Deifalla, A.; Hamed, M.; Saleh, A.; Ali, T. Exploring GFRP bars as reinforcement for rectangular and L-shaped beams subjected to significant torsion: An experimental study. Eng. Struct. 2014, 59, 776–786.
16. Deifalla, A.F.; Zapris, A.G.; Chalioris, C.E. Multivariable Regression Strength Model for Steel Fiber-Reinforced Concrete Beams under Torsion. Materials 2021, 14, 3889. https://doi.org/10.3390/ma14143889.
17. Deifalla, K.M.S.; Abdelrahman, A. Simplified Model for the Torsional Strength of Concrete Beams with GFRP Stirrups. J. Compos. Constr. 2015, 19, 04014032. https://doi.org/10.1061/(ASCE)CC.1943-5614.0000498.
18. Ebid, A.; Deifalla, A. Prediction of Shear Strength of FRP Reinforced Beams with and Without Stirrups Using (GP) Technique. Ain Shams Eng. J. 2021, 12, 2493–2510. https://doi.org/10.1016/j.asej.2021.02.006.
19. Hassan, M.M.; Deifalla, A. Evaluating the new CAN/CSA-S806-12 torsion provisions for concrete beams with FRP reinforcements. Mater. Struct. 2016, 49, 2715–2729. https://doi.org/10.1617/s11527-015-0680-9.
20. Salem, N.M.; Deifalla, A. Evaluation of the Strength of Slab–Column Connections with FRPs Using Machine Learning Algorithms. Polymers 2022, 14, 1517. https://doi.org/10.3390/polym14081517.
21. Deifalla, A.; Awad, A.; El-Garhy, M. Effectiveness of Externally Bonded CFRP Strips for Strengthening Flanged Beams under Torsion: An Experimental Study. Eng. Struct. 2013, 56, 2065–2075.
22. Deifalla, A.; Ghobarah, A. Full torsional behavior of RC beams wrapped with FRP: Analytical model. Compos. Constr. 2010, 14, 289–300.
23. Deifalla, A.; Ghobarah, A. Strengthening RC T-Beams Subjected to Combined Torsion and Shear Using FRP fabrics—Experimental study. Compos. Constr. 2010, 14, 301–311.
24. fib Task group 5.1. FIB Bulletin 90, Externally applied FRP reinforcement for concrete structures. Lausanne, Switzerland: 2019.
25. ACI Committee 440. ACI 440.2R-17, Guide for the Design and Construction of Externally Bonded FRP Systems for Strengthening Concrete Structures. Farmington Hills, Michigan, USA: 2017.
26. Construction C– AC on TR for. CNR-DT 200 R1/2013 Guide for the Design and Construction of Externally Bonded FRP Systems for Strengthening Existing Structures. Rome, Italy: 2013.
27. TR-55 CSTR. Design guidance for strengthening concrete structures using fiber composite materials. London, Great Britain: 2012.
28. JSCE Japanese Society of Civil Engineers. Recommendations for upgrading of concrete structures with use of continuous fiber sheets; 2000.

29. Bousselham A, Chaallal O. Behavior of reinforced concrete t-beams strengthened in shear with carbon fiber-reinforced polymer-an experimental study. ACI Struct J 2006; 103:339–47.
30. Bousselham A, Chaallal O. Mechanisms of shear resistance of concrete beams strengthened in shear with externally bonded FRP. J Compos Constr 2008; 12:499–512. https://doi.org/10.1061/(ASCE)1090-0268(2008)12:5(499).
31. Chen GM, Teng JG, Chen JF, Rosenboom OA. Interaction between steel stirrups and shear strengthening FRP strips in RC beams. J Compos Constr 2010; 14:498–509. https://doi.org/10.1061/(ASCE)CC.1943-5614.0000120.
32. Pellegrino C, Modena C. Fiber reinforced polymer shear strengthening of reinforced concrete beams with transverse steel reinforcement. J Compos Constr 2002; 6:104–11. https://doi.org/10.1061/(ASCE)1090-0268(2002)6:2.
33. Pellegrino C, Vasic M. Assessment of design procedures for the use of externally bonded FRP composites in shear strengthening of reinforced concrete beams. Compos Part B Eng 2013; 45:727–41. https://doi.org/10.1016/j.compositesb.2012.07.039.
34. Sas G, Täljsten B, Barros J, Lima J, Carolin A. Are available models reliable for predicting the FRP contribution to the shear resistance of RC beams. Journal of Compositses for Construction 2009; 13:514–34. https://doi.org/10.1061/(ASCE)CC.1943-5614.0000045.
35. Mofidi A, Chaallal O. Tests and Design Provisions for Reinforced-Concrete Beams Strengthened in Shear Using FRP Sheets and Strips. Int J Concr Struct Mater 2014; 8:117–28. https://doi.org/10.1007/s40069-013-0060-1.
36. Mofidi A, Chaallal O. Shear strengthening of RC beams with externally bonded FRP composites: effect of strip-width-to-strip-spacing ratio. J Compos Constr 2011; 15:732–42. https://doi.org/10.1061/(ASCE)CC.1943-5614.0000219.
37. Mofidi A, Chaallal O. Shear Strengthening of RC Beams with EB FRP: Influencing Factors and Conceptual Debonding Model. J Compos Constr 2011; 15:62–74. https://doi.org/10.1061/(ASCE)CC.1943-5614.0000153.
38. Kalfat R, Al-Mahaidi R, Smith S. Anchorage devices used to improve the performance of reinforced concrete beams retrofitted with FRP composites: state-of-the-art review. Journal Composites for Construction, 2013;17(1):14–33.
39. Godat A. Hammad F., Chaallal O. State-of-the-art review of anchored FRP shear-strengthened RC beams: A study of influencing factors. 2020. Composite Structures 254 (2020) 112767.
40. Ebid, A.; Deifalla, A. Using Artificial Intelligence Techniques to Predict Punching Shear Capacity of Lightweight Concrete Slabs. Materials 2022, 15, 2732. https://doi.org/10.3390/ma15082732.
41. Deifalla, A.; Salem, N.M. A Machine Learning Model for Torsion Strength of Externally Bonded FRP-Reinforced Concrete Beams. Polymers **2022**, 14, 1824. https://doi.org/10.3390/polym14091824.
42. Colotti V, Swamy RN. Unified analytical approach for determining shear capacity of RC beams strengthened with FRP. Eng Struct 2011; 33:827–42.
43. Sas G, Täljsten B, Barros J, Lima J, Carolin A. Are available models reliable for predicting the FRP contribution to the shear resistance of RC beams? J Compos Constr 2009; 13:514–34. https://doi.org/10.1061/(ASCE)CC.1943-5614.0000045.
44. Kotynia R, Oller E, Mari AR, Kaszubska M. Efficiency of shear strengthening of RC beams with externally bonded FRP materials – State-of-the-art in the experimental tests. Compos Part B Eng n.d.
45. Abuodeh, Omar R., Jamal A. Abdalla, and Rami A. Hawileh. Prediction of shear strength and behavior of RC beams strengthened with externally bonded FRP sheets using machine learning techniques. Composite Structures 234 (2020): 111698.